UAV-based Advanced Remote Sensing of the Polar Regions

2020. 1. 31

PURDUE UNIVERSITY

Submission

To: Chief of Korea Polar Research Institute

This report is submitted as the final report of entrusted research "UAV-based Advanced Remote Sensing of the Polar Regions" project of "Antarctic subglacial topography (BEDMAP) survey using unmanned system" project.

2020. 1. 31

(Main Project) Person in charge of Entire Research: Joohan Lee

Name of Entrusted Organization: Purdue University

Entrusted Researcher in charge: Melba Crawford

Participating Entrusted Researchers: Ali Masjedi

" : John Evan Flatt

Summary

Low-cost unmanned aerial vehicles (UAVs) utilizing push-broom hyperspectral scanners are poised to become a popular alternative to conventional remote sensing platforms such as manned aircraft and satellites. In order to employ this emerging technology in fields, direct georeferencing of hyperspectral data using onboard integrated global navigation satellite systems (GNSSs) and inertial navigation systems (INSs) is required. Directly deriving the scanner position and orientation requires the spatial and rotational relationship between the coordinate systems of the GNSS/INS and hyperspectral scanner to be measured. The spatial offset (lever arm) between the scanner and GNSS/INS unit can be measured manually. However, the angular relationship (boresight angles) between the scanner and GNSS/INS coordinate systems, which is more critical for accurate generation of georeferenced products, is difficult to establish. This study presents three calibration approaches to estimate the boresight angles relating hyperspectral push-broom scanner and GNSS/INS coordinate systems. For reliable /practical estimation of the boresight angles, this study starts with establishing the optimal/minimal flight and control/tie point configuration through a bias impact analysis starting from the point positioning equation. Then, an approximate calibration procedure utilizing tie points in overlapping scenes is presented after making some assumptions about the flight trajectory and topography of covered terrain. Next, two rigorous approaches are introduced – one using ground control points and other using tie features. The approximate/rigorous approaches are based on enforcing the collinearity and coplanarity of the light rays connecting the perspective centers of the imaging scanner, object point, and the respective image points.

Table of Contents

KOPRI 극지연구소

UAV-based Advanced Remote Sensing of the Polar Regions

1. Introduction

In many of today's rapidly growing technological and industrial fields, hyperspectral imaging is quickly emerging as an irreplaceable mechanism for collecting high-quality scientific data. By measuring the spectral radiance in narrow bands across large swaths of the electromagnetic spectrum, hyper–spectral sensors or imaging spectrometers are able to provide large amounts of characteristic information pertaining to the objects they capture. The growing popularity of hyperspectral imaging technology and recent advances in unmanned aerial vehicles (UAVs) created an environment where high-resolution hyperspectral imaging is more accessible than ever. Hyperspectral imaging has been adopted to a considerable extent in precision agricultural applications [1], [2]. Precision agriculture employs phenotypic data to improve management of farm inputs, such as fertilizers, herbicides, seed, and fuel [3]. Phenotypic data captured by hyper-spectral sensors enables researchers and agronomists to sense crop characteristics such as moisture content, nutrients, chlorophyll, leaf area index, and crop biomass without the drawbacks associated with laborious and expensive in-field measurements [4].

In the past, hyperspectral imaging utilized mobile mapping systems (MMS), such as satellites and manned aircrafts as the platforms for agricultural data collection. Modern MMS including terrestrial and airborne platforms provide economic and accurate means to collect data for urban mapping, environmental monitoring, transportation planning, change detection, resource management, and precision agriculture [5]. Due to recent improvements in the accuracy of integrated Global Navigation Satellite Systems (GNSSs) and inertial navigation systems (INS), an MMS can now provide georeferenced data with high spatial accuracy. For agricultural management applications, the increased requirements for geospatial data at a higher spatial resolution and temporal frequency made it clear that manned aircraft and satellite remote sensing systems cannot fully satisfy such needs.

Therefore, low-cost UAVs are emerging as ideal alternative platforms for agricultural management [6]. UAVs offer several design and performance advantages over other conventional platforms, such as small size, low weight, low flying height, slow flight speed, low cost, and ease of storage and deployment [7], [8]. A UAV-based MMS is capable of providing high spatial resolution data at a higher data collection rate. Meanwhile, integrated GNSS/INS mounted on a UAV allows for directly georeferencing the acquired data with high accuracy while eliminating the need for an excessive number of ground control points (GCPs).

With regard to deriving accurate three-dimensional (3-D) geospatial information from 2-D hyperspectral scenes, the interior and exterior orientation of the utilized sensor should be established. Interior orientation, which encompasses the internal sensor characteristics such as focal length and lens distortion, is established through a sensor calibration procedure. Exterior orientation, which defines the position and orientation of the scanner at the moment of exposure, is traditionally established using GCPs within a bundle adjustment procedure. Nowadays, with the help of an integrated GNSS/INS unit onboard, the exterior orientation parameters can be directly estimated without the need for GCPs [9]–[11]. Due to the large volume of acquired data by a hyperspectral scanner, high spatial resolution systems are usually based on having a 1-D array along the focal plane while operating through what is commonly known as "push-broom scanning mechanism." A push-broom scanner acquires a thin strip at a given exposure. A scene is formed by successive exposures along the flight trajectory and concatenating the acquired strips [12]. Considering that the exterior orientation parameters of every scan line have to be determined, a direct georeferencing procedure is usually adopted to provide the position and orientation of the scanner using an integrated GNSS/INS unit. In this regard, one should note that the GNSS/INS position and orientation refer to the body frame of the inertial measurement unit (IMU). Therefore, the lever arm components and boresight angles between the hyperspectral push-broom scanner and IMU body frame coordinate systems need to be estimated to derive accurate position and orientation of the scanner. The lever arm denoting the spatial displacement between the IMU body frame and the perspective center of the scanner can be established to a reasonable accuracy (e.g., 2–3 cm) using conventional measurements tools [13]. However, boresight angles relating the IMU body frame and the scanner coordinate systems can only be roughly established. The boresight angles play more critical role than the lever arm components in controlling the geospatial accuracy of derived products due to the error propagation of the former with the platform height. Thus, reliable boresight angles calibration is essential for ensuring the spatial accuracy of GNSS/INS-assisted imaging platforms.

2. Theoretical background

Boresight calibration approaches of frame imaging sensors through bundle adjustment of overlapping images along and across the flight direction together with several GCPs are well established [14]–[16]. For push-broom scanners, significant research has been dedicated toward establishing reliable boresight calibration strategies. Muller et al. [17] proposed a boresight calibration approach for airborne and space borne push-broom scanners. In that approach, the boresight angles were estimated by minimizing the difference between the ground coordinates of GCPs and the projected ground coordinates of the respective image points. More specifically, using the interior orientation parameters, GNSS/INS geo-referencing parameters, nominal lever arm components, and boresight angles, and an available digital elevation model (DEM), the image points corresponding to established GCPs were projected onto the DEM using a ray tracing procedure. Then, boresight angles were estimated by minimizing the differences between the GCPs and the projected ground coordinates. The experimental dataset in this paper was acquired by the push-broom scanner "ROSIS-03" over a test site from a flying height of 3230 m. An IGI AeroControl CCNS IIb was used for the determination of platform position and orientation. The accuracy of the GNSS/INS position and orientation information is about 0.1–0.3mand 0.01°–0.1°, respectively. Using a DEM with 5–10 m vertical accuracy and 25 m horizontal resolution, five GCPs were used for boresight calibration. The estimated ground coordinates of seven check points were compared to the surveyed coordinates to evaluate the accuracy of the boresight calibration procedure. The RMSE of the differences in the XY coordinates was around 1.5 m, which is almost at the same level as the ground sampling distance (GSD) of the used sensor (1.9 m).

Based on the conceptual basis of the approach proposed by Muller et al. [17], similar strategies involving additional parameters (e.g., aircraft stabilizer scaling factors and variations of sensor's CCD size) in the calibration procedure were discussed in Yeh and Tsai [18] and Zhang et al. [19]. In these approaches, the achieved accuracy for the orthorectified mosaics using the estimated boresight angles and a given DEM were found to be accurate at the level of the GSD of the involved sensors. Lenz et al. [20] proposed an automated in-flight boresight calibration approach for push-broom scanners. The boresight angles were estimated by forcing conjugate light rays to intersect as much as possible. The proposed approach applied speeded up robust features (SURF) detector to identify interest points, whose descriptors were used in a matching routine to derive homologous points in overlapping scenes. Then, tie points were projected onto a DEM utilizing a ray tracing algorithm using nominal values for the boresight angles. The boresight angles were derived by minimizing the root-mean-square error between the ground coordinates of corresponding tie points. The approach was evaluated using two dataset with overlapping strips over a forested mountain and a relatively flat urban area, where the average GSD was 0.5 m for both dataset. To evaluate the boresight calibration results, residual errors were calculated using a reference dataset comprised of manually defined tie points. The RMSE of the residual errors was 1.5 m (three times the GSD) for the forest dataset and 0.5 m (GSD level) for the urban area. The key limitation of the above approaches is the need for having a DEM of the covered area as well as some GCPs. Moreover, none of the previous literature addressed the optimal/minimal flight and control/tie point configuration for reliable estimation of the boresight angles. In response to these limitations, this study starts with an investigation of the optimal/minimal configuration of the flight and control/tie point layout for reliable/practical boresight calibration through bias impact analysis. The analysis is based on evaluating the impact of incremental changes in the boresight pitch, roll, and heading angles ($\delta\Delta\omega$, $\delta\Delta\phi$, and $\delta\Delta\kappa$) on derived ground coordinates after making some assumptions regarding the flight trajectory and topography of the covered terrain (e.g., parallel scanner and IMU coordinate systems and vertical scanner over relatively flat/horizontal terrain). The derived impact is then used to establish an optimal/minimal flight and control/tie point configuration for reliable boresight angles estimation. An approximate approach that starts with the outcome of the bias impact analysis is then introduced for evaluating the boresight angles using tie features in overlapping scenes. Afterward, two rigorous approaches are presented. The first one is based on using GCPs in single or multiple flight lines. The second rigorous approach estimates the boresight angles using tie points only.

3. Point positioning

The developed strategies for bias impact analysis and boresight calibration are based on the collinearity equations, which describe the conceptual basis of point positioning using GNSS/INS-assisted push-broom scanners. A push-broom scanner system involves three coordinate systems—a mapping frame, an IMU body frame, and a scanner frame. The mathematical model of the collinearity principle—which describes the collinearity of the scanner perspective center, image point, and corresponding object point—is graphically illustrated and mathematically introduced in Fig. 1 and (1), respectively. The notations for spatial offsets and rotations used in Fig. 1 and (1) are as follows: First, r_a^b denotes the spatial offset for point *a* relative to a coordinate system associated with point *b*; and second, R_a^bdenotes the rotation matrix that transforms a vector from coordinate system *a* to coordinate system *b*. The superscripts/subscripts *m*, *b*, and *c* represent the mapping, IMU body frame, and camera/scanner coordinate systems, respectively. In (1), r_I^m represents ground coordinates of the object point *I*; $r_b^m(t)$ and $R_b^m(t)$ are the GNSS/INS-based position and orientation information of the IMU body frame coordinate system relative to the mapping frame; r_c^b and R_c^b are the lever arm vector and boresight rotation matrix relating the push-broom scanner and IMU body frame coordinate systems; r_i^c denotes the vector connecting the scanner perspective center to the image point, *i*, corresponding to an object point, *I*; and λ_i is a point-specific unknown scale factor that varies with the terrain relief and scanner tilt. As illustrated in Fig. 1, one can define the xyz-axes of the scanner coordinate system to be aligned across flight, along flight, and up directions, respectively. In the case of push-broom scanners, the y-image coordinates for any point would be constant, which depends on the scanner alignment along the focal plane. Usually, the scan line is set vertically below the perspective center of the used lens—thus making the y-image coordinate almost zero. The y-scene coordinate defines the time of the exposure for the scan line in question. Starting with (1), one can perform the boresight bias impact analysis for a push-broom scanner as

$$r_I^m = r_b^m(t) + R_b^m(t)\, r_b^m + \lambda_i R_b^m(t)\, R_c^b r_i^c \tag{1}$$

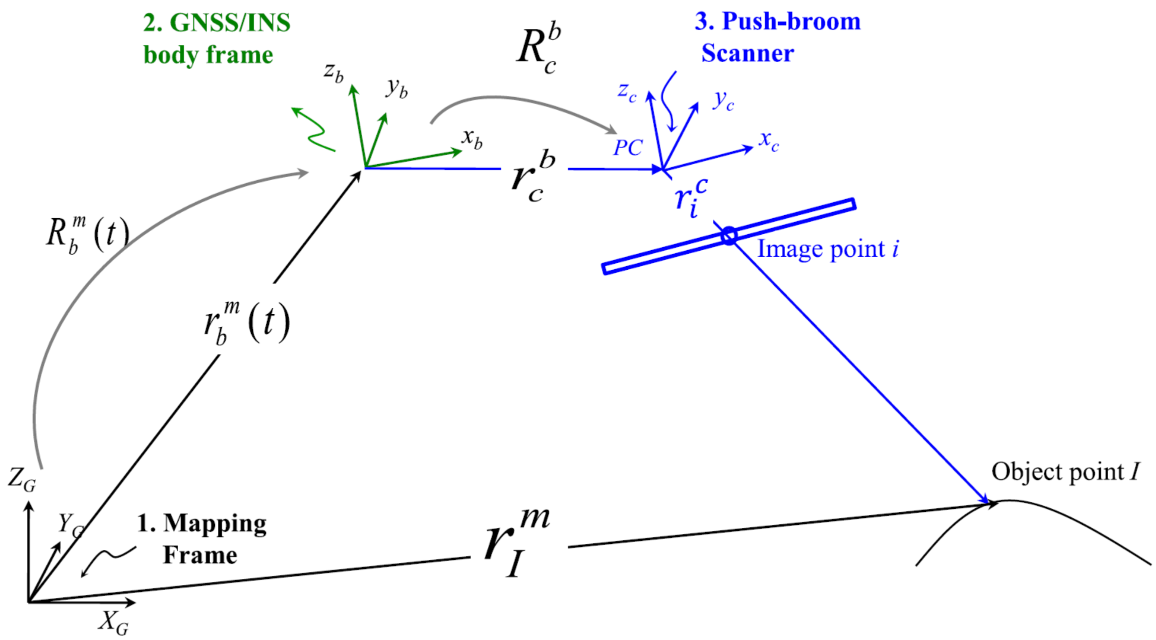

Fig. 1. Schematic diagram of the collinearity equations and definition of the coordinate systems for a push-broom scanner.

4. Bias impact analysis for boresight angles

As discussed in the introduction section, the boresight angles for a GNSS/INS-assisted push-broom scanner are usually determined with the help of a DEM together with a set of GCPs. In this research, the boresight angles will be determined using either a set of GCPs or tie features that are manually identified in overlapping push-broom scanner scenes. Automated extraction of GCPs and/or tie features will be the focus of future research. When using GCPs, the boresight estimation strategy aims at ensuring the collinearity of the GCP, corresponding image point, and perspective center of the scan line encompassing the image point. When relying on tie features, the boresight angle estimation strategy enforces the intersection of the light rays connecting the perspective centers of the scan lines encompassing corresponding image points of the tie feature and the respective conjugate image points. In other words, the calibration target function aims at estimating the boresight angles that ensures the coplanarity of conjugate image features and the respective perspective centers for the scan lines where these image points are identified. An optimal flight and control/tie point configuration is the one that will exhibit large deviations from the respective target functions (i.e., collinearity or coplanarity) due to small changes in the boresight angles. Therefore, the optimal flight and control/tie point configuration can be set only after analyzing the impact of biases in the boresight angles on the collinearity/coplanarity target functions. Such bias impact can be established by considering the collinearity equations and evaluating the changes in the ground coordinates of derived object points as a result of biases in the boresight angles. Evaluating the bias impact on derived ground coordinates is directly related to the GCP-based approach since the bias impact will violate the collinearity objective. On the other hand, the impact on the ground coordinates is indirectly related to the tie feature-based approach since the bias impact on the ground coordinates will also cause deviations from the coplanarity of corresponding light rays associated with the image points for the tie feature in question. To facilitate straightforward analysis of the bias impact, we will make some assumptions regarding the system setup, flight trajectory, and topography of the covered area. More specifically, we will be making the following assumptions:

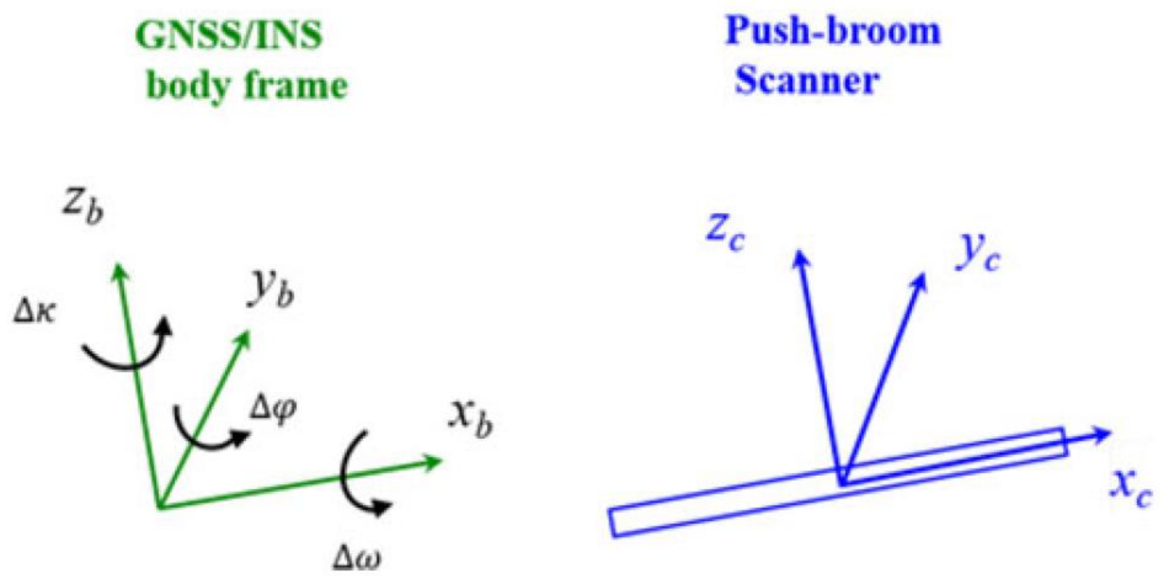

Fig. 2. Alignment of the scanner and IMU body frame coordinate systems.

1) The IMU is setup in the platform with its x-, y-, and z- axes pointing in the starboard, forward, and up directions, respectively.
2) The z-axis of the IMU coordinate system is aligned along the vertical direction (i.e., the ω and φ angles of the $R_b^m(t)$ rotation matrix are zeros).
3) The platform is traveling in the South-to-North (denoted as forward) and North-to-South (denoted as backward) directions while maintaining a constant heading. Thus, the κ angles for the forward and backward directions will be 0° and 180°, respectively.
4) The push-broom scanner coordinate system is almost parallel to the IMU body frame (i.e., the angular offsets between these coordinate systems—Δω, Δφ, and Δκ—are within ±5°), as shown in Fig. 2.
5) The push-broom scanner is flying at a constant elevation while covering a relatively flat terrain.

Assumptions 2 and 3 would result in $R_b^m(t)$ being defined according to (2.a), where the top and bottom signs refer to the forward and backward flight directions, respectively. Assumption 4 would lead to a boresight matrix R_c^b that is defined by the incremental rotation in (2.b), where Δω, Δφ, and Δκ represent the boresight pitch, roll, and heading angles, respectively. One should note that the above assumptions are only introduced to facilitate the bias impact analysis. The findings of the analysis would still apply regardless of the flight directions, IMU alignment, push-broom scanner alignment relative to the IMU body frame, flying height variation, and nature of covered terrain unless it is explicitly stated in the forthcoming boresight angles estimation strategies

$$R_b^m(t) = \begin{bmatrix} \pm 1 & 0 & 0 \\ 0 & \pm 1 & 0 \\ 0 & 0 & 1 \end{bmatrix} \tag{2.a}$$

$$R_c^b = \begin{bmatrix} 1 & -\Delta\kappa & \Delta\varphi \\ \Delta\kappa & 1 & -\Delta\omega \\ -\Delta\varphi & \Delta\omega & 1 \end{bmatrix} \tag{2.b}$$

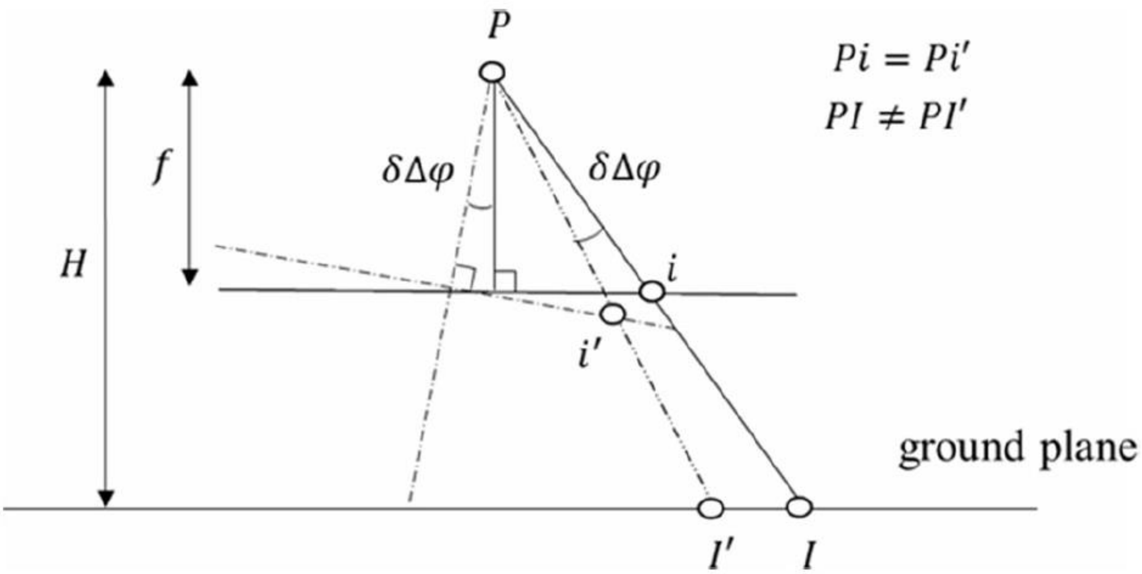

Fig. 3. Impact of variation in the boresight roll angle (δΔφ) on the scale factor λ_i for a push-broom scanner.

극지연구소

Following the above assumptions, the point positioning equation for a push-broom scanner would reduce to the form in (3), where once again the top and bottom signs refer to the forward and backward flight directions, respectively. In (3), $[\Delta X\ \Delta Y\ \Delta Z]^T$ represents the lever arm vector relating the IMU body frame and scanner while $[\boldsymbol{x_i} \quad \boldsymbol{0} \quad \boldsymbol{-f}]^{\boldsymbol{T}}$ represents the vector $\boldsymbol{r_i^c}$ connecting the perspective center and the image point in question (with f being the focal length). Using (3.c), one can derive the impact of a bias in the boresight angles on the ground coordinates of the derived object point through partial derivatives w.r.t. the boresight pitch, roll, and heading angles and its multiplication with assumed biases (namely, δΔω, δΔφ, and δΔκ). Before proceeding with such analysis, one should note that owing to the push-broom scanning mechanism, a variation in the boresight roll angle (Δφ) will result in a tilt of the scan line relative to the covered terrain, thus leading to a variation in the scale factor ($\boldsymbol{\lambda_i}$) along the scan line, as shown in Fig. 3. Alternatively, variations in boresight pitch (Δω) and boresight heading (Δκ) angles will not affect the scale factor as the scan line would still remain parallel to the terrain. Therefore, the dependence of the scale factor ($\boldsymbol{\lambda_i}$) on the boresight roll angle (Δφ) should be considered within the bias impact analysis

$$r_I^m = r_b^m(t) + \begin{bmatrix} \pm\Delta X \\ \pm\Delta Y \\ \Delta Z \end{bmatrix} + \begin{bmatrix} \pm 1 & 0 & 0 \\ 0 & \pm 1 & 0 \\ 0 & 0 & 1 \end{bmatrix} \begin{bmatrix} 1 & -\Delta\kappa & \Delta\varphi \\ \Delta\kappa & 1 & -\Delta\omega \\ -\Delta\varphi & \Delta\omega & 1 \end{bmatrix} \begin{bmatrix} x_i \\ 0 \\ -f \end{bmatrix} \tag{3.a}$$

$$r_I^m = r_b^m(t) + \begin{bmatrix} \pm\Delta X \\ \pm\Delta Y \\ \Delta Z \end{bmatrix} + \lambda_i \begin{bmatrix} \pm 1 & \mp\Delta\kappa & \Delta\varphi \\ \pm\Delta\kappa & \pm 1 & \mp\Delta\omega \\ -\Delta\varphi & \Delta\omega & 1 \end{bmatrix} \begin{bmatrix} x_i \\ 0 \\ -f \end{bmatrix} \tag{3.b}$$

$$r_I^m = r_b^m(t) + \begin{bmatrix} \pm\Delta X \\ \pm\Delta Y \\ \Delta Z \end{bmatrix} + \lambda_i \begin{bmatrix} \pm x_i \mp f\Delta\varphi \\ \pm x_i\Delta\kappa \pm f\Delta\omega \\ -x_i\Delta\varphi - f \end{bmatrix} \tag{3.c}$$

Starting with the simplified collinearity, (3.c), the impact of variation in the boresight pitch angle (δΔω) can be presented by (4), where the scale factor is approximated as $\lambda_i = H/f$, owing to the assumption of having a vertical scanner over relatively flat terrain. Similarly, the impact of variation in the boresight heading angle (δΔκ) can be given by (5). X'_I in (5) represents the lateral distance, while considering the appropriate sign, between the object point and the flight trajectory. One should note that for a given object point, x_i and X'_I will change their sign depending on the flying direction, as shown in Fig. 4.

$$\delta r_I^m(\delta\Delta\omega) = \lambda_i \begin{bmatrix} 0 \\ \pm f\delta\Delta\omega \\ 0 \end{bmatrix} = \begin{bmatrix} 0 \\ \pm H\delta\Delta\omega \\ 0 \end{bmatrix} \tag{4}$$

$$\delta r_I^m(\delta\Delta\kappa) = \lambda_i \begin{bmatrix} 0 \\ \pm \mathrm{x}_i\delta\Delta\kappa \\ 0 \end{bmatrix} = \begin{bmatrix} 0 \\ \pm X'_I\delta\Delta\kappa \\ 0 \end{bmatrix} \tag{5}$$

where $X'_I = \lambda_i x_i \approx \frac{H}{f} x_i$.

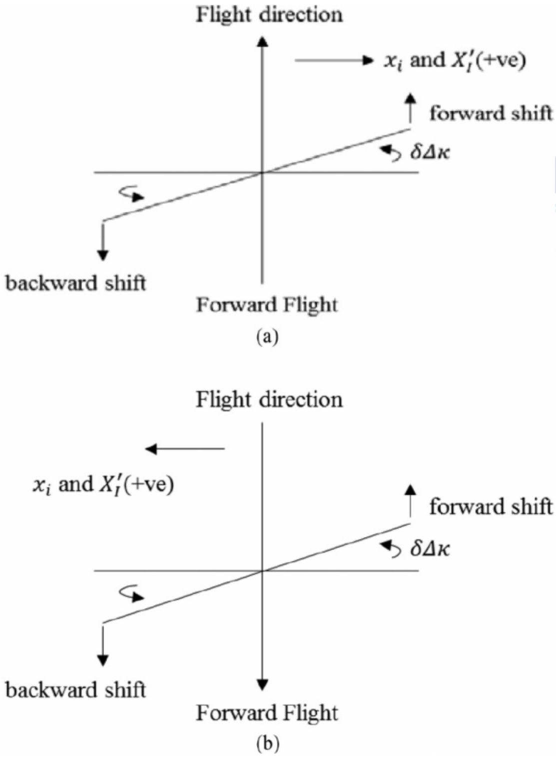

Fig. 4. Impact of variation in the boresight heading angle on ground coordinates.

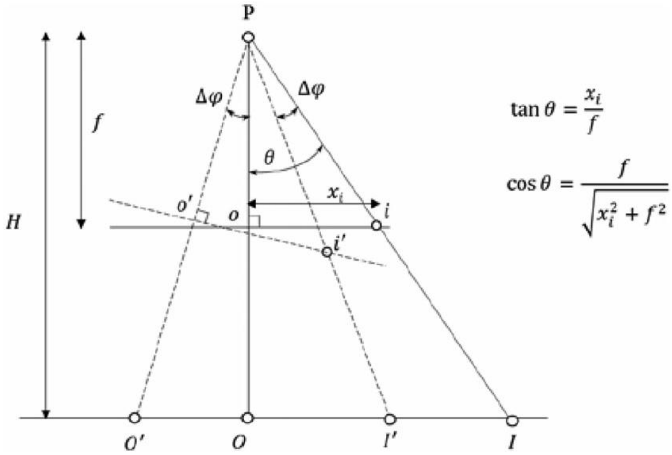

Fig. 5. Incremental change in the scale factor due to the variation in the boresight roll angle.

For the impact of variation in the boresight roll angle (δΔφ), one should also consider the impact of such variation on the scale factor. Thus, the combined impact on the ground coordinates can be represented by (6), which, in turn, could be expanded to (7) after replacing $\frac{\partial\lambda_i}{(\partial\Delta\varphi)}\delta\Delta\varphi$) with $\delta\lambda_i(\delta\Delta\varphi)$. Considering that the boresight angles and the impact of boresight roll angle variation on the scale factor— $\delta\lambda_i(\delta\Delta\varphi$—are small values, the second order incremental terms in (7) (in bold) can be ignored. Thus, (7) could be reduced to the form in (8). To simplify (8) further, the impact of variation in the boresight roll on the scale factor ($\delta\lambda_i(\delta\Delta\varphi)$) can be derived with the help of Fig. 5. For a vertical scanner, given an image point *i* and corresponding object point *I*, the scale factor can be defined as $\lambda_i = \frac{PI}{Pi} = \frac{H}{f}$, where *P* denotes the perspective center of the push-broom scanner. As can be seen in Fig. 5, the scale factor as a function of the boresight roll angle (Δφ) is represented by (9), where the term $\cos(\theta - \Delta\varphi)$ can be expanded according to (10) while assuming small boresight roll angle Δφ. As per Fig. 5, the distance *PI'* can be derived according to (11). Since$\mathrm{Pi'} = Pi = (f^2 + x_i^2)^{0.5}$, the scale factor as a function of the boresight roll angle (Δφ) can be represented by (12). As a result, the change in the scale factor due to incremental change in the boresight roll angle can be derived, (13). Finally, the impact of incremental change in the boresight roll angle $(\delta\Delta\varphi)$ on the ground coordinates can be presented by (14), where X'_I is the lateral distance between the object point and flight trajectory.

$$\delta r_I^m(\delta\Delta\varphi) = \lambda_i \begin{bmatrix} \pm f\delta\Delta\varphi \\ 0 \\ -x_i\delta\Delta\varphi \end{bmatrix} + \frac{\partial\lambda_i}{(\partial\Delta\varphi)}\delta\Delta\varphi \begin{bmatrix} \pm x_i \mp f\Delta\varphi \\ \pm x_i\Delta\kappa \pm f\Delta\omega \\ -x_i\Delta\varphi - f \end{bmatrix} \tag{6}$$

$$\delta r_I^m(\delta\Delta\varphi) = \lambda_i \begin{bmatrix} \pm f\delta\Delta\varphi \\ 0 \\ -x_i\delta\Delta\varphi \end{bmatrix} + \begin{bmatrix} \pm x_i\delta\lambda_i(\delta\Delta\varphi) \mp f\Delta\varphi\delta\lambda_i(\delta\Delta\varphi) \\ \pm x_i\Delta\kappa\delta\lambda_i(\delta\Delta\varphi) \pm f\Delta\omega\delta\lambda_i(\delta\Delta\varphi) \\ -x_i\Delta\varphi\delta\lambda_i(\delta\Delta\varphi) - f\delta\lambda_i(\delta\Delta\varphi) \end{bmatrix} \tag{7}$$

$$\delta r_I^m(\delta\Delta\varphi) = \lambda_i \begin{bmatrix} \pm f\delta\Delta\varphi \\ 0 \\ -x_i\delta\Delta\varphi \end{bmatrix} + \begin{bmatrix} \pm x_i\delta\lambda_i(\delta\Delta\varphi) \\ 0 \\ -f\delta\lambda_i(\delta\Delta\varphi) \end{bmatrix} \tag{8}$$

$$\lambda'_i(\Delta\varphi) = \frac{PI'}{Pi'} = \frac{PI'}{(f^2 + x_i{}^2)^{0.5}}, \textit{where } \mathrm{PI'} = \frac{\mathrm{H}}{\cos(\theta - \Delta\varphi)} \tag{9}$$

$$\cos(\theta - \Delta\varphi) = \cos\theta\cos\Delta\varphi + \sin\theta\sin\Delta\varphi \cong \cos\theta + \Delta\varphi\sin\theta \tag{10}$$

$$\mathrm{PI}' = \frac{H}{\cos\theta + \sin\theta\Delta\varphi} = \frac{H/\cos\theta}{1+\tan\theta\Delta\varphi} \cong \frac{H}{\cos\theta}(1-\tan\theta\Delta\varphi) \tag{11.a}$$

$$\mathrm{PI}' = \frac{H}{\frac{f}{\left(f^2+x_i^2\right)^{0.5}}}\left(1-\frac{x_i}{f}\Delta\varphi\right) \tag{11.b}$$

$$\lambda'_i(\Delta\varphi) = \frac{H}{f}\left(1-\frac{x_i}{f}\Delta\varphi\right) = \frac{H}{f} - \frac{H}{f^2}x_i\Delta\varphi \tag{12}$$

$$\delta\lambda_i(\delta\Delta\varphi) = \frac{H}{f^2}x_i\delta\Delta\varphi \tag{13}$$

$$\delta r_I^m(\delta\Delta\varphi) = \lambda_i\begin{bmatrix}\mp f\delta\Delta\varphi \\ 0 \\ -x_i\delta\Delta\varphi\end{bmatrix} + \begin{bmatrix}\pm x_i\left(-\frac{H}{f^2}\right)x_i\delta\Delta\varphi \\ 0 \\ -f\left(-\frac{H}{f^2}\right)x_i\delta\Delta\varphi\end{bmatrix} \tag{14.a}$$

$$r_I^m(\delta\Delta\varphi) = \begin{bmatrix}\mp H\delta\Delta\varphi \mp \frac{{X'_I}^2}{H}\delta\Delta\varphi \\ 0 \\ -X'_I\delta\Delta\varphi + X'_I\delta\Delta\varphi\end{bmatrix} = \begin{bmatrix}\mp\left(H+\frac{{X'_I}^2}{H}\right)\delta\Delta\varphi \\ 0 \\ 0\end{bmatrix} \tag{14.b}$$

According to the above bias impact analysis, the total impact of boresight angle variations on the ground coordinates is given by (15). Based on that equation, one can state the following:

1) A bias in the boresight pitch angle $(\delta\Delta\omega)$ will impact the coordinates along the flight direction. The impact of this bias on the ground coordinates depends on the platform's flying height and flying direction.

2) A bias in the boresight roll angle $(\delta\Delta\varphi)$will impact the coordinates across the flight direction. The impact of this bias on the ground coordinates depends on flying height, flight direction, and lateral distance between the point in question and the flight trajectory.

3) A bias in the boresight heading $(\delta\Delta\kappa)$will impact the coordinates along the flight direction. The impact of such variation on the ground coordinates is flying direction independent (as the impact of the $\pm$ signs will be nullified by the sign of the lateral distance—X'_I —when flying in different directions). The impact increases as the lateral distance between the control/tie feature in question and trajectory increases. For control/tie features that are directly below the flight trajectory (i.e., x_i and $X'_I \cong 0$), then $\delta r_I^m(\delta\Delta\kappa) \cong 0$, which implies that the boresight heading angle cannot be estimated if the control/tie features are aligned along the center of the swath covered by the push-broom scan line.

$$\delta r_I^m(\delta\Delta\omega,\delta\Delta\varphi,\delta\Delta\kappa) = \begin{bmatrix}\mp\left(H+\frac{{X'_I}^2}{H}\delta\Delta\varphi\right) \\ \pm H\delta\Delta\omega \pm X'_I\delta\Delta\kappa \\ 0\end{bmatrix} \tag{15}$$

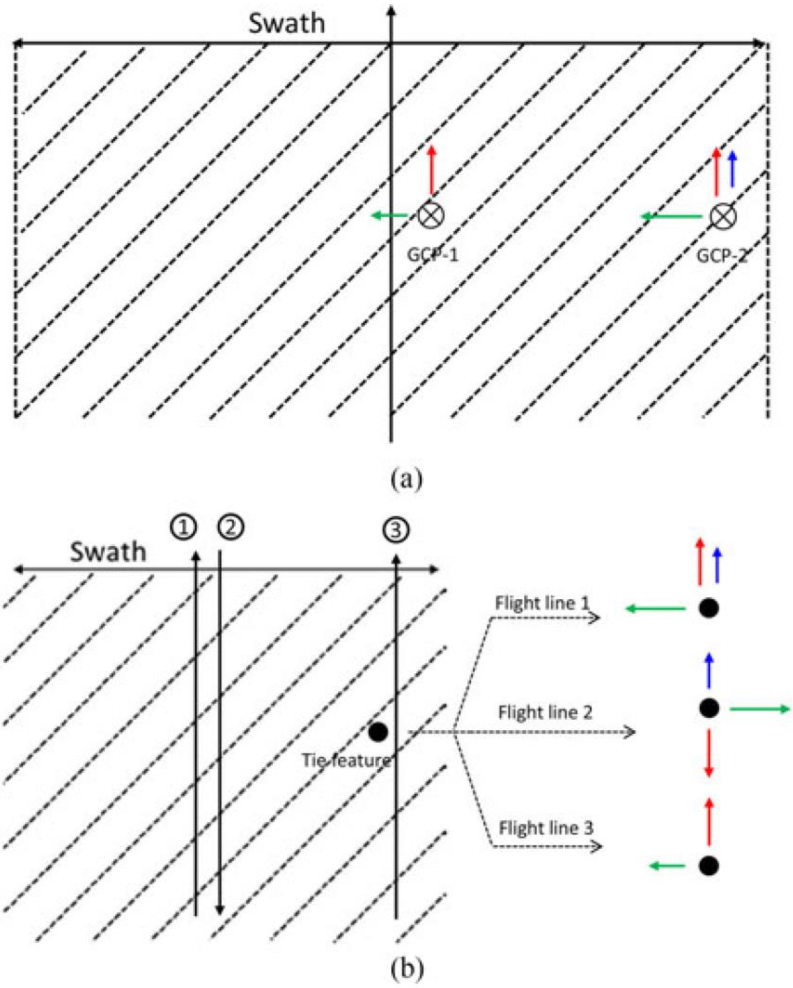

Fig. 6. Optimal/minimal flight configuration for (a) a GCP-based approach and (b) a tie-feature-based approach, where the red, green, and blue arrows represent the impact of a bias in the boresight pitch, roll, and heading angles ($\delta\Delta\omega, \delta\Delta\varphi, \delta\Delta\kappa$), respectively. The dashed areas represent the swath covered by the central flight line(s).

Based on the above findings, the optimal/minimal configuration of flight lines and control/tie points for the estimation of the boresight angles can be summarized as follows:

1) For a GCP-based approach, a single flight line and two GCPs—with one aligned along the center of the covered swath and the other point aligned along the edge of the covered swath—are needed [see Fig. 6(a)]. The GCP aligned along the swath center will allow for the estimation of the boresight pitch and roll angles ($\Delta\omega$ and $\Delta\varphi$) by minimizing the discrepancies along and across the flight line (the impact of the boresight heading angle at that point would be quite minimal). The point at the edge of the swath will allow for the estimation of the boresight heading angle ($\Delta\kappa$).

2) For a tie feature-based approach, three flight lines and a single tie feature would be needed. Two of the flight lines should be in opposite directions and have 100% overlap. The third flight line should be parallel to one of the first two with an overlap of roughly 50%. The tie point could be located along the center of the scan covered by the third flight line [see Fig. 6(b)]. Enforcing the coplanarity of the light rays associated with the identified tie point in the opposite scans with 100% overlap would allow for the estimation of the boresight pitch and roll angles ($\Delta\omega$ and $\Delta\varphi$)—one should note that

since the impact of a bias in the boresight heading is flying direction independent, ($\delta\Delta\kappa$) will not impact the coplanarity of the conjugate light rays for those flight lines. On the other hand, enforcing the coplanarity of the light rays associated with the identified tie point in the parallel flight lines with 50% overlap will ensure the estimation of the boresight heading angle ($\Delta\kappa$).

In practice, it is recommended to use more GCPs/tie point features to derive an estimate of the evaluated boresight angles while minimizing the impact of random errors in the system measurements as well as improve the ability to detect gross errors in such measurements (i.e., improving the reliability of the adjustment procedure).

5. Boresight calibration strategies

In this section, we start by introducing an approximate calibration procedure utilizing tie points in overlapping scenes. This procedure is based on the previously discussed bias impact analysis. Then, two rigorous approaches, which use GCPs and tie features, are introduced. As mentioned earlier, the approximate and rigorous approaches are based on enforcing the collinearity and coplanarity of light rays connecting the perspective centers of the imaging scanner, object point, and the respective image points.

A. Approximate boresight calibration using tie features

First, we propose an approximate boresight calibration strategy, which is based on the use of tie features and some of the stated assumptions for the bias impact analysis. More specifically, the boresight angles are estimated by enforcing the intersection of the light rays connecting the perspective centers of the scan lines encompassing the corresponding image points of the tie feature and the respective conjugate image points (i.e., enforcing the coplanarity constraint). To relax the requirement for having almost parallel IMU and scanner coordinate systems (i.e., we are always dealing with small boresight angles), one can introduce a virtual scanner coordinate system—denoted byc'—that is almost parallel to the original scanner frame—denoted by c. The boresight matrix relating the virtual scanner, c', to the IMU body frame $R^b_{c'}$can be set by the user to represent the nominal relationship between the scanner and IMU body frame coordinate systems. Therefore, the boresight rotation matrix R^b_c can be decomposed into two rotation matrices as $R^b_c = R^b_{c'} R^{c'}_{c'}$ where $R^{c'}_c$is an unknown incremental boresight rotation matrix that is defined by incremental boresight pitch, roll, and heading angles($\Delta\omega$,$\Delta\varphi$, $\Delta\kappa$). Thus, the collinearity equations can be represented by the form in (16). Another assumption that could be relaxed is the one related to having a push-broom scanner, which is flown along the South-to-North and North-to-South directions. In cases where the flight lines do not adhere to this assumption, one can manipulate the trajectory position and orientation ($r^m_b(t) and\ R^m_b(t)$)) information so they are defined relative to a mapping frame that is parallel to the flight directions. After such manipulation, the rotation matrix ($R^m_{c'}(t)$) will take the form in (2.a). At this stage, it worth mentioning that the decomposition of the boresight matrix also eliminates the need for having the IMU body frame axes aligned along the starboard, forward, and up directions since we will be working with $R^m_{c'}(t)$ rather than $R^m_b(t)$

$$r^m_I = r^m_b(t) + R^m_b(t)\, r^b_c + \lambda_i R^m_{c'}(\mathrm{t}) R^{c'}_c\, r^c_i \qquad (16)$$

where $R^m_{c'}(t) = R^m_b(t)\, R^b_{c'}$.

Following the above assumption relaxation procedure, we are only left with the strict requirements for having almost vertical scanner over a relatively flat terrain. For an identified tie point in multiple flight lines, the derived ground coordinates using the nominal values for the boresight angles (i.e., assuming $\Delta\omega, \Delta\varphi, \Delta\kappa$to be zeros) can be derived according to (17). So, for a tie point in overlapping scenes, the difference between the estimated ground coordinates from the respective flight lines—denoted as a and b—could be represented by (18), where X'_a and X'_b represent the lateral distance between the corresponding object point and the a and b flight trajectories. If a tie feature is captured in n image strips, one of them is regarded as a reference and the remaining (n − 1) occurrences are paired with it to produce (n − 1) set of equations of the form in (18). Using a flight and tie point configuration that meets the stated layout in Fig. 6(b), we will have four equations (of the form in (18)) from the formulated pairs—the Z-difference between the projected points will not be used as they are not related to biases in the incremental boresight angles—in three unknowns. Thus, these equations can be used in least squares adjustment (LSA) to solve for biases in the boresight angles $\delta\Delta\omega, \delta\Delta\varphi,$ and $\delta\Delta\kappa$. Since this approach estimates biases in the boresight angles, the boresight angles defining the matrix $R_c^{c'}$ will be $-\delta\Delta\omega, -\delta\Delta\varphi,$ and $-\delta\Delta\kappa$. Finally, the boresight rotation matrix R_c^b is derived by multiplying the nominal boresight rotation matrix $\mathrm{R}_{c'}^b$ and the incremental boresight matrix $(\mathrm{R}_c^{c'})$, which is defined by $(-\delta\Delta\omega, -\delta\Delta\varphi, \text{and} -\delta\Delta\kappa)$

$$r_I^m(estimated) = r_I^m(true) + \delta r_I^m(\delta\Delta\omega, \delta\Delta\varphi, \delta\Delta\kappa)$$
$$= r_I^m(true) + \begin{bmatrix} \mp\left(H + \frac{{X'_I}^2}{H}\right)\delta\Delta\varphi \\ \pm H\delta\Delta\omega \pm X'_I\delta\Delta\kappa \\ 0 \end{bmatrix} \quad (17)$$

$$r_I^m(a, estimated) - r_I^m(b, estimated) = \begin{bmatrix} \mp\left(H + \frac{{X'_a}^2}{H}\right)\delta\Delta\varphi \\ \pm H\delta\Delta\omega \pm X'_a\delta\Delta\kappa \\ 0 \end{bmatrix} - \begin{bmatrix} \mp\left(H + \frac{{X'_b}^2}{H}\right)\delta\Delta\varphi \\ \pm H\delta\Delta\omega \pm X'_b\delta\Delta\kappa \\ 0 \end{bmatrix} \quad (18)$$

B. Rigorous boresight calibration using GCPs

In this section, we present a rigorous boresight calibration procedure that uses identified GCPs in the acquired push-broom hyperspectral scenes. The proposed procedure is based on a reformulated collinearity equation model where the image coordinates are represented as a function of the GNSS/INS position and orientation, ground coordinates of the GCP, lever arm components, and the boresight angles as represented by (19). To avoid running into the gimbal lock problem (i.e., the secondary rotation angle of R_c^b is 90°), the boresight matrix R_c^b is decomposed into the product of two rotation matrices $R_{c'}^b$ and $R_c^{c'}$ —where ***c'*** represents a virtual scanner. Similar to the approximate approach, the virtual scanner coordinate system ***c'*** is set up to be almost parallel to the original scanner coordinate system ***c***. In such a case, $R_{c'}^b$ will be a known rotation matrix that depends on the alignment of the scanner relative to the IMU body frame and $R_c^{c'}$ will be defined by the unknown incremental rotation in (2.b). Therefore, (19) could be reformulated to the form in (20), which can be simplified as in (21). One should note that $[N_X N_Y D]^T$ in (21) is fully defined by the measured image coordinates, internal characteristics of the scanner, GNSS/INS position and orientation information, lever arm components, and nominal boresight matrix ($R_{c'}^b$). To eliminate the unknown scale factor λ_i from (21), the first and second rows can be divided by the third one to produce (22), which is nonlinear in the unknown boresight angles $(\Delta\omega, \Delta\varphi, \Delta\kappa)$.

Adopting a similar approach to the direct linear transformation [21], this nonlinear relationship can be re-expressed in a linear form as per (23). For each image point corresponding to a given GCP, two equations in three unknowns can be derived. Having a minimal configuration similar to the one represented by Fig. 6(a), four equations can be formulated and used to solve for the incremental boresight angles defining $R_c^{c'}$, which could be used to derive the boresight matrix R_c^b as the product of $R_{c'}^b$ and $R_c^{c'}$

$$r_i^c = \frac{1}{\lambda_i} R_c^b \{R_m^b(t)[r_I^m - r_b^m(t)] - r_c^b\} \tag{19}$$

$$r_i^c = \frac{1}{\lambda_i} R_{c'}^c R_b^{c'} \{R_m^b(t)[r_I^m - r_b^m(t)] - r_c^b\} \tag{20}$$

$$r_i^c = \frac{1}{\lambda_i} \begin{bmatrix} 1 & -\Delta\kappa & \Delta\varphi \\ \Delta\kappa & 1 & -\Delta\omega \\ -\Delta\varphi & \Delta\omega & 1 \end{bmatrix} \begin{bmatrix} N_X \\ N_Y \\ D \end{bmatrix}$$
$$\text{where } \begin{bmatrix} N_X \\ N_Y \\ D \end{bmatrix} = R_b^{c'} \{R_m^b(t)[r_I^m - r_b^m(t)] - r_c^b\} \tag{21}$$

$$\frac{x_i}{-f} = \frac{N_X - N_Y \Delta\kappa + \mathrm{D}\Delta\varphi}{-N_X \Delta\varphi + N_Y \Delta\omega + D} \tag{22.a}$$

$$\frac{y_i}{-f} = \frac{N_X \Delta\kappa + N_Y - \mathrm{D}\Delta\omega}{-N_X \Delta\varphi + N_Y \Delta\omega + D} \tag{22.b}$$

$$x_i(-N_X \Delta\varphi + N_Y \Delta\omega + D) = -f(N_X - N_Y \Delta\kappa + \mathrm{D}\Delta\varphi) \tag{23.a}$$

$$y_i(-N_X \Delta\varphi + N_Y \Delta\omega + D) = -f(N_X \Delta\kappa + N_Y - \mathrm{D}\Delta\omega) \tag{23.b}$$

C. Rigorous boresight calibration using tie features

Rather than using GCPs, this approach is based on using identified tie features in the push-broom scanner scenes to estimate the boresight angles. As stated earlier, the boresight angles are estimated by enforcing the coplanarity constraint relating conjugate features in overlapping push-broom hyperspectral scenes. Similar to the previous approach, situations leading to a gimbal lock could be mitigated by introducing a virtual scanner—***c'***—that is almost parallel to the original scanner and using a known nominal boresight rotation matrix ($R_{c'}^b$) relating the IMU body frame and the virtual scanner coordinate systems. Therefore, the unknown boresight angles would be the incremental angles ($\Delta\omega, \Delta\varphi, \Delta\kappa$) defining $R_c^{c'}$. The used mathematical model is the one represented by (22), where both the incremental boresight angles (($\Delta\omega, \Delta\varphi, \Delta\kappa$)) and the ground coordinates of the tie features r_I^m are unknowns. Since one is dealing with a nonlinear model in the involved unknowns, an iterative LSA procedure should be used starting from approximate values of the unknowns. For the incremental boresight angles, $\Delta\omega, \Delta\varphi$, and $\Delta\kappa$ can be assumed to be zeros. This assumption is quite valid since we are solving for the rotational relationship between the original and virtual scanner coordinate systems. The approximate values for the ground coordinates of the tie features can be derived using (16) while assuming vertical imagery over relatively flat terrain (thus, the scale factor can be approximated by the ratio between the flying height above ground and the scanner principal distance, i.e.,$\lambda_i = \frac{H}{f}$). Using the optimal/minimal flight and tie point configuration suggested by Fig. 6(b), one will have six equations in six unknowns; namely the incremental boresight angles and the ground coordinates of the tie feature in question. One should note that using more flight lines and/or tie features are highly recommended. Similar to the previous calibration strategies, the boresight rotation matrix (R_c^b) is derived by multiplying the nominal boresight rotation matrix ($R_{c'}^b$) and the incremental boresight matrix ($R_c^{c'}$).

6. Conclusion

Potential advances in push-broom hyperspectral scanners and GNSS/INS position and orientation systems will lead to improved geospatial products only after accurate estimation of the mounting parameters relating the different sensors. Due to the widespread popularity of low-cost UAVs and the demands of nontraditional applications such as agricultural management, there is pressing need for reliable and practical estimation of the mounting parameters, in general, and boresight angles, in particular, relating the GNSS/INS unit to the scanner coordinate systems. To ensure reliable/practical estimation of the boresight angles, this research started with a bias impact analysis to derive the optimal/minimal flight and control/tie point configuration for the estimation of the boresight angles. The conceptual basis of the bias impact analysis is deriving the flight configuration that maximizes the impact of biases in the boresight parameters while ensuring the sufficiency of the flight and control/tie feature configuration to avoid any potential correlation among the sought after parameters. More specifically, the analysis has shown that the optimal/minimal flight and control/tie point configuration should encompass: First, flight lines in opposite and/or parallel directions and second, GCPs or tie features that are laterally displaced from the flight lines. The research then proceeds by introducing different calibration strategies. The first approach is an approximate one and uses tie features in overlapping scenes to estimate the boresight angles after making some assumptions regarding the flight trajectory and topography of the covered area (namely, vertical imagery over relatively flat terrain). The other two approaches are rigorous with one using GCPs while the other relying on tie points. The GCP-based rigorous approach aims at minimizing the differences between the projected object points onto the image space and the observed image points for the used GCPs (i.e., enforcing the collinearity principle). The tie-feature-based rigorous approach is aims to improve the intersection of conjugate light rays corresponding to tie features (i.e., enforcing the coplanarity principle)

7. References

[1] D.Haboudane, J.R.Miller,E. Pattey, P. J. Zarco-Tejada, and I.B. Strachan, “Hyperspectral vegetation indices and novel algorithms for predicting green LAI of crop canopies: Modeling and validation in the context of precision agriculture,” *Remote Sens. Environ.*, vol. 90, no. 3, pp. 337–352, 2004.

[2] A. McBratney, B. Whelan, T. Ancev, and J. Bouma, “Future directions of precision agriculture,” *Precis. Agriculture*, vol. 6, no. 1, pp. 7–23, 2005.

[3] R. K. Crookston, “A top 10 list of developments and issues impacting crop management and ecology during the past 50 years,” *Crop Sci.*, vol. 46, no. 5, pp. 2253–2262, 2006.

[4] D. J.Mulla, “Twenty five years of remote sensing in precision agriculture: Key advances and remaining knowledge gaps,” *Biosyst. Eng.*, vol. 114, no. 4, pp. 358–371, 2013.

[5] C. V. Tao and J. Li, *Advances in Mobile Mapping Technology*, vol. 4. Boca Raton, FL, USA: CRC Press, 2007.

[6] A. Habib, Y. Han, W. Xiong, F. He, Z. Zhang, and M. Crawford, “Automated ortho-rectification of UAV-based hyperspectral data over an agricultural field using frame RGB imagery,” *Remote Sens.*, vol. 8, no. 10, 2016, Art. no. 796.

[7] S. R. Herwitz *et al.*, “Imaging from an unmanned aerial vehicle: Agricultural surveillance and decision support,” *Comput. Electron. Agriculture*, vol. 44, no. 1, pp. 49–61, 2004.

[8] A. Habib, W. Xiong, F. He, H. L. Yang, and M. Crawford, “Improving orthorectification of UAV-Based push-broom scanner imagery using derived orthophotos from frame cameras,” *IEEE J. Sel. Topics Appl. Earth Observ. Remote Sens.*, vol. 10, no. 1, pp. 262–276, Jan. 2017.

[9] M. Cramer, D. Stallmann, and N. Haala, “Direct georeferencing using GPS/inertial exterior orientations for photogrammetric applications,” *Int. Arch. Photogrammetry Remote Sens.*, vol. 33, no. B3/1, part 3, pp. 198–205, 2000 .

[10] N. Pfeifer, P. Glira, and C. Briese, “Direct georeferencing with on board navigation components of light weight UAV platforms,” *Int. Arch. Photogrammetry, Remote Sens. Spatial Inf. Sci.*, vol. 39-B7, pp. 487–492, 2012.

[11] A. S. Elsharkawy and A. F. Habib, “Error Analysis for the Airborne Direct Georeferincing Technique,” *Int. Arch. Photogrammetry, Remote Sens. Spatial Inf. Sci.*, vol. XLI-B1, pp. 1213–1219, 2016.

[12] R. Gupta and R. I. Hartley, “Linear pushbroom cameras,” *IEEE Trans. Pattern Anal. Mach. Intell.*, vol. 19, no. 9, pp. 963 975, Sep. 1997.

[13] J. Skaloud andD. Lichti, “Rigorous approach to bore-sight self-calibration in airborne laser scanning,” *ISPRS J. Photogrammetry Remote Sens.*, vol. 61, no.1, pp. 47–59, 2006.

[14] M. M. Mostafa and K.-P. Schwarz, “Digital image georeferencing from a multiple camera system by GPS/INS,” *ISPRS J. Photogrammetry Remote Sens.*, vol. 56, no. 1, pp. 1–12, 2001.

[15] A. Habib, A. Kersting, K. Bang, and J. Rau, “A novel single-step procedure for the calibration of the mounting parameters of a multi-camera terrestrial mobile mapping system,” *Archiwum Fotogrametrii, Kartografiii Teledetekcji*, vol. 22, pp. 173 185, 2011.

[16] A. P.Kersting, A. Habib, andK. I.Bang, “Mounting parameters calibration of GPS/INS-assisted photogrammetric systems,” in *Proc. 2011 Int. Workshop Multi-Platform/Multi-Sensor Remote Sens. Mapping*, 2011, pp. 1–6.

[17] R. Muller, M. Lehner, R. Muller, P. Reinartz, M. Schroeder, and B.Vollmer, “A program for direct georeferencing of airborne and spaceborne line scanner images,” *Int. Arch. Photogrammetry Remote Sens. Spatial Inf. Sci.*, vol. 34, no. 1, pp. 148–153, 2002.

[18] C.-K. Yeh and V. J. Tsai, “Direct georeferencing of airborne pushbroom images,” *J. Chin. Inst. Eng.*, vol. 38, no. 5, pp. 653–664, 2015.

[19] A. Zhang, S. Hu, X. Meng, L. Yang, and H. Li, “Toward high altitude airship ground-based boresight calibration of hyperspectral pushbroom imaging sensors,” *Remote Sens.*, vol. 7, no. 12, pp. 17297–17311, 2015.

[20] A. Lenz, H. Schilling, D. Perpeet, S. Wuttke, W. Gross, and W. Middelmann, “Automatic in-flight boresight calibration considering topography for hyperspectral pushbroom sensors,” in *Proc. 2014 IEEE Int. Geosci. Remote Sens. Symp.*, 2014, pp. 2981–2984.

[21] Y. I. Abdel-Aziz, “Direct linear transformation from comparator coordinates in close-range photogrammetry,” in *Proc. Amer. Soc. Photogrammetry Symp. Close-Range Photogrammetry*, Falls Church, VA, USA, 1971, pp. 1–19.

KOPRI 극지연구소

Warning

1. This report is a report of research results of a project entrusted by the Korea Polar Research Institute.

2. When you present the contents of this report, you must state that these contents are research results of a project entrusted by the Korea Polar Research Institute.

3. Materials concerning the nation's classified science and technology information must not be presented or disclosed.